J|A|C|S
ARTICLES
Published on Web 10/12/2004

Computer Simulation of Solid and Liquid Benzene with an Atomistic Interaction Potential Derived from ab Initio Calculations

Ivo Cacelli, Giorgio Cinacchi, Giacomo Prampolini, and Alessandro Tani*

Contribution from the Dipartimento di Chimica e Chimica Industriale, Università di Pisa, via Risorgimento 35, I-56126 Pisa, Italy

Received June 8, 2004; E-mail: tani@dcci.unipi.it

Abstract: Molecular dynamics atomistic simulations of solid and liquid benzene have been performed, employing a model intermolecular potential derived from quantum mechanical calculations. The ab initio database includes approximately 200 geometries of the benzene dimer with interaction energies computed at the MP2 level of theory. The accuracy of the modeled force field results is satisfactory. The thermodynamic and structural properties, calculated in the condensed phases, are compared with experimental data and previous simulation results. Single particle and collective dynamical properties are also investigated through the calculation of translational and rotational diffusion coefficients, reorientational dynamics, and viscosities. The agreement of these data with experimental measurements confirms the reliability of the proposed force field.

1. Introduction

Computer simulation methods, such as Monte Carlo (MC) and molecular dynamics (MD), have proven to be powerful tools for studying the bulk properties of condensed phases, ranging from simple liquids to complex materials, such as liquid crystals or polymers.[1,2] When the goal is the "realistic" modeling of a given molecular system, an accurate description of the interactions among the particles is required. Two main approaches have been pursued in the construction of the force fields.

The most widely[3−6] employed scheme is based on an a posteriori strategy. In this approach, the set of parameters specifying the force field is adjusted in order to reproduce some target macroscopic properties, such as the experimental density or the vaporization enthalpy. Although capable of excellent results, this kind of scheme suffers from some disadvantages.

(i) The parameter optimization procedure rapidly becomes very costly in terms of both human resources and computational time as the molecular size increases. For this reason, the interaction potential has to be described with few parameters, and only simplified atom−atom functions, such as Lennard-Jones (LJ), can be considered. This lack of flexibility might undermine the possibility for the modeled intermolecular potential to be close to the exact two-body interaction energy.

(ii) Since the target experimental properties refer to a given pressure and temperature, good results are, in general, guaranteed only in a limited range of these thermodynamic variables.

(iii) The interaction potential is an "effective" potential in the sense that it embodies not only the predominant two-body effects but also the many-body effects. Even though they generally resemble two-body energies, their physical description is, in principle, weak.

(iv) The extension of such force fields to large molecules can be done only by assuming the parameters transferability. Unfortunately, in complex materials, it is well-known that small differences in the molecular structure may produce impressive variations in the macroscopic properties, and transferability must be used with caution.

The other possible approach for constructing efficient force fields consists of deriving the model potential from first principle calculations. A number of quantum mechanical (QM) calculations for a set of representative intermolecular geometries are carried out to model a simplified potential, which will be used in simulations. Due to the high computational requirement of accurate QM calculations, this alternative scheme has been less widely used, with some important exceptions (e.g., water,[7] methanol, and acetonitrile).[8] Nevertheless, it presents several advantages that can be summarized as follows.

(i) The ab initio-derived interaction potentials are not driven by experimental data. This allows the construction of force

(1) Allen, M.; Tildesley, D. *Computer Simulation of Liquids*; Clarendon Press: Oxford, U.K., 1987.
(2) Frenkel, D.; Smith, B. *Understanding Molecular Simulations*; Academic Press: San Diego, CA, 1996.
(3) Brooks, B. R.; Bruccoleri, R. E.; Olafson, B. D.; States, D. J.; Swaminanthan, S.; Karplus, M. *J. Comput. Chem.* **1983**, *4*, 187.
(4) Hermans, J.; Berendsen, H.; van Gunsteren, W.; Postma, J. *Biopolymers* **1984**, *23*, 1.
(5) Cornell, W. D.; Cieplak, P.; Bayly, C. I.; Gould, I. R.; Merz, K. M.; Ferguson, D. M.; Spellmeyer, D. C.; Fox, T.; Caldwell, J. W.; Kollmann, P. A. *J. Am. Chem. Soc.* **1995**, *117*, 5179.
(6) Jorgensen, W. L.; Maxwell, D. S.; Tirado-Rives, J. *J. Am. Chem. Soc.* **1996**, *118*, 11225.
(7) Xantheas, S. S. Intermolecular interactions and cooperative effects from electronic structure calculations: an effective means for developing interaction potentials for condensed phase simulations. In *Novel Approaches to the Structure and Dynamics of Liquids: Experiments, Theories, and Simulation*; Samios, J., Durov, V., Eds.; Kluwer: Dodrecht, The Netherlands, 2004.
(8) Sum, R. B. A. K.; Sandler, S. I.; Szalewicz, K. *J. Chem. Phys.* **2002**, *116*, 7627.

10.1021/ja046642u CCC: $27.50

fields, even for molecules whose properties are difficult to measure, and in principle, gives the approach predictive capabilities for all molecules.

(ii) This interaction potential has a well-defined physical meaning in the sense that it is a real two-body intermolecular energy. This knowledge allows the computation of the second virial coefficient to be performed, which can be compared with experimental data without running computer simulations. Three-body contribution may be, in principle, calculated, as well, and included in the construction of the force field in a direct or average way.

(iii) The force field is tailored on the chosen molecule and, therefore, takes into account the details of a specific chemical structure. No degree of transferability must be invoked for such interaction potentials.

(iv) The ab initio-computed potential energy surface (PES) constitutes a reference database for the parametrization through a fitting procedure of model potentials of different complexity and realism. This chance appears to be important in large molecules, where a full atomic representation can be computationally too expensive and simplified models are to be used.[9]

The corresponding disadvantages are the following.

(i) The ab initio-computed PESs may show very complex shapes, which cannot be well fitted through the standard full atomic force fields. However, this problem can be solved by introducing more flexible model potentials, specified by a larger number of parameters, but still suitable for computer simulations.

(ii) The sampling of the PES can be computationally very expensive, in particular, for those molecules whose low spatial symmetry requires the energy evaluation of many geometries. The difficulty in establishing a criteria for the completeness of the sampling is a further subtle problem.

(iii) The ab initio calculation of the accurate intermolecular energies of dimers through standard QM techniques quickly becomes not feasible with the increasing of molecular dimensions. However, to circumvent this problem, we have recently proposed a fragmentation−reconstruction method (FRM),[10] which allows an accurate estimate of the interaction energy of large molecules. From our point of view, this second route appears more appealing, and exploiting the rapid increase of computational resources, we believe it is worthwhile of further pursuit. With this aim, we report in this work the results of the molecular simulation of benzene whose interaction potential has been modeled by a large set of QM calculations.

The benzene molecule has been chosen for several reasons. First, benzene has been extensively studied, both from a theoretical[11−24] and an experimental[25−37] point of view, thus making a comparison of many different properties possible. Several other atomistic model potentials, obtained from quantum mechanical calculations only[12,13] or calibrated on experimental measures,[15,18−21] can be found in the literature, and most of them yield accurate results with regard to the properties of liquid benzene at room temperature. Much less attention has been given to the capability of these models to represent the crystal−liquid transition, which becomes crucial in fields such as liquid crystals or polymers. Moreover, from a theoretical point of view, the benzene dimer constitutes a demanding test for ab initio calculations since a correct representation of the dispersion interaction requires careful calibration of both the basis set and the method employed.[16,17,22] Finally, an accurate sampling of the benzene dimer's PES can lead (through the FRM)[10] to the construction of the interaction potential of large molecules containing the benzene fragment.[9,38]

The present paper is organized as follows. The next section provides computational details of the ab initio calculations, the employed model potential, and the simulation technique. In Results and Discussion, the model intermolecular PES computation and the simulation runs are discussed. Conclusions are made at the end of the paper.

2. Methods

2.1. Ab Initio Calculations. To obtain reliable interaction energies in van der Waals' complexes, one has to choose a method that includes a significant fraction of the electronic correlation energy. In fact, HF computations fail dramatically in predicting bonded structures of benzene and other aromatic pairs.[22] This is essentially due to the lack of dispersion energy (always attractive), which is expected to be crucial in molecules with electron delocalization, such as aromatic molecules.

In view of the large number of configurations required to provide a significant representation of the six-dimensional potential energy surfaces of the dimer, $E(X,Y,Z,\alpha,\beta,\gamma)$, and of the necessity to include the basis set superposition error correction,[39] we have looked for a reasonable compromise between accuracy and computational requirements. We have used the second-order perturbative theory in the Möller−Plesset scheme coupled with a double-ζ plus polarization basis set, originally proposed by Hobza et al.[17] This basis differs from the

(9) Cacelli, I.; Cinacchi, G.; Prampolini, G.; Tani, A. Computer simulation of mesogens with ab initio interaction potentials. In *Novel Approaches to the Structure and Dynamics of Liquids: Experiments, Theories, and Simulation*; Samios, J., Durov, V., Eds.; Kluwer: Dodrecht, The Netherlands, 2004.
(10) Amovilli, C.; Cacelli, I.; Campanile, S.; Prampolini, G. *J. Chem. Phys.* **2002**, *117*, 3003.
(11) Claessens, M.; Ferrario, M.; Ryckaert, J. *Mol. Phys.* **1983**, *50*, 217.
(12) Linse, P. *J. Am. Chem. Soc.* **1984**, *106*, 5425.
(13) Linse, P.; Engström, S.; Jönsson, B. *Chem. Phys. Lett.* **1985**, *115*, 95.
(14) Shi, X.; Bartell, L. *J. Phys. Chem.* **1988**, *92*, 5667.
(15) Jorgensen, W.; Severance, D. *J. Am. Chem. Soc.* **1990**, *112*, 4768.
(16) Smith, G. D.; Jaffe, R. L. *J. Phys. Chem.* **1996**, *100*, 9624.
(17) Hobza, P.; Selzle, H. L.; Schlag, E. W. *J. Phys. Chem.* **1996**, *100*, 18790.
(18) Cabaço, M.; Danten, Y.; Besnard, M.; Guissani, Y.; Guillot, B. *J. Phys. Chem. B* **1997**, *101*, 6977.
(19) Errington, J. R.; Panagiotopoulos, A. Z. *J. Chem. Phys.* **1999**, *111*, 9731.
(20) Chelli, R.; Cardini, G.; Procacci, P.; Righini, R.; Califano, S.; Albrecht, A. *J. Chem. Phys.* **2000**, *113*, 6851.
(21) Witt, R.; Sturz, L.; Dölle, A.; Müller-Plathe, F. *J. Phys. Chem. A* **2000**, *104*, 5716.
(22) Tsuzuki, S.; Honda, K.; Uchimaru, T.; Mikami, M.; Tanabe, K. *J. Am. Chem. Soc.* **2002**, *124*, 104.
(23) Cacelli, I.; Cinacchi, G.; Prampolini, G.; Tani, A. *J. Chem. Phys.* **2004**, *120*, 3648.
(24) Ryu, S.; Stratt, R. M. *J. Phys. Chem. B* **2004**, *108*, 6782.
(25) Timmermans, J. *Physico-chemical Constants of Pure Organic Compounds*; Elsevier: New York, 1950.
(26) Bacon, G.; Curry, N.; Wilson, S. *Proc. R. Soc. London, Ser. A* **1964**, *279*, 98.
(27) Falcone, D.; Douglass, D.; McCall, D. *J. Phys. Chem.* **1967**, *71*, 2754.
(28) Dymond, J.; Smith, E. *The Virial Coefficients of Gases and Mixtures: A Critical Compilation*; Clarendon Press: Oxford, U.K., 1969.
(29) Landolt-Börnstein. *Zahlenwerte und Funktionen, Band II, Teil 5, Transport Phänomene;* Springer: Berlin, 1969.
(30) Tanabe, K. *Chem. Phys. Lett.* **1979**, *63*, 43.
(31) Smith, G. *Mol. Cryst. Liq. Cryst.* **1979**, *49*, 207.
(32) Battaglia, M.; Buckingham, A.; Williams, J. *Chem. Phys. Lett.* **1981**, *78*, 421.
(33) Majer, V.; Svoboda, V. *Enthalpies of Vaporization of Organic Compounds: A Critical Review and Data Compilation*; Blackwell Scientific Publications: Oxford, U.K., 1985.
(34) Grolier, J.; Roux-Desgranges, G.; Berkane, M.; Jimenez, E.; Wilhelm, E. *J. Chem. Thermodyn.* **1993**, *25*, 41.
(35) Klüner, R. *Rotatorische Dynamik von Kohlenwasserstoffen in flüssiger Phase*; Shaker-Verlag: Aachen, Germany, 1995.
(36) *Handbook of Chemistry and Physics*; Lide, D. R., Ed.; CRC Press: Boca Raton, FL, 1997.
(37) Linde, B. B. J.; Lezhnev, N. *Ultrasonics* **2000**, *38*, 945.
(38) Bizzarri, M.; Cacelli, I.; Prampolini, G.; Tani, A. *J. Phys. Chem. A* **2004**, in press.
(39) Boys, S. F.; Bernardi, F. *Mol. Phys.* **1970**, *19*, 553.

standard 6-31G* basis set for the low exponent of the Gaussian-type d orbitals that are centered on the carbon atoms ($\alpha_d = 0.28$), which was calibrated with the help of more-sophisticated and time-consuming theoretical results.[10] Its ability to give reliable results in a relatively inexpensive way was already tested in a previous work,[23] where a comparison with the results of Tsuzuki et al.[22] (probably the most-accurate theoretical results in the literature) shows energy differences that are less than 0.2 kcal/mol.

2.2. Model Intermolecular Potentials. The benzene molecule was modeled by placing an interaction site on each atom. The employed site−site potential, u_{ij}, is a modified version of the well-known 12-6 Lennard-Jones potential, with a Coulombic contribution, for example

$$u_{ij} = 4\epsilon_{ij}\left[\left(\frac{\xi_{ij}\sigma_{ij}}{r_{ij} - (\xi_{ij} - 1)\sigma_{ij}}\right)^{12} - \left(\frac{\xi_{ij}\sigma_{ij}}{r_{ij} - (\xi_{ij} - 1)\sigma_{ij}}\right)^{6}\right] + \frac{q_i q_j}{r_{ij}} \quad (1)$$

where i and j represent the two interaction sites whose distance is r_{ij}. The parameter (ξ) was added to improve the flexibility of the fitting, allowing the width of the interaction energy curve to vary independently from its depth. The interaction parameters of unlike pairs (ϵ_{ij}, σ_{ij}, and ξ_{ij}) were obtained through the following mixing rules:

$$\epsilon_{ij} = (\epsilon_i\epsilon_j)^{1/2}; \qquad \sigma_{ij} = \frac{(\sigma_i + \sigma_j)}{2}; \qquad \xi_{ij} = (\xi_i\xi_j)^{1/2} \quad (2)$$

The database containing approximately 200 benzene−benzene ab initio interaction energies,[23] $E(X,Y,Z,\alpha,\beta,\gamma)$, was fitted through a nonlinear minimization routine[40] to an intermolecular model potential:

$$U(X,Y,Z,\alpha,\beta,\gamma) = \sum_{i=1}^{12}\sum_{j=1}^{12} u_{ij}(r_{ij}) \quad (3)$$

where u_{ij} is the site−site potential defined in eq 1. The fitting procedure was performed by looking for the minimum, with respect to the set of seven independent parameters, $\mathbf{A} = \{\epsilon_i, \sigma_i, \xi_i, q_i\}$, of the function:

$$I(\mathbf{A}) = \frac{\sum_{k=1}^{N_{geom}} \omega_k [E_k - U_k(\mathbf{A})]^2}{\sum_{k=1}^{N_{geom}} \omega_k} \quad (4)$$

where the index, k, specifies the geometry of the benzene dimer, and the ω_k values are the appropriate weights. During the fitting, no constraint was imposed on the parameters, except those dictated by the spatial symmetry and electroneutrality of the molecule. Thus, the independent parameters were ϵ_C, σ_C, ξ_C, q_C, ϵ_H, σ_H, and ξ_H. The root-mean-square (RMS) error was estimated as RMS $= \sqrt{I}$.

The set of five independent parameters, $\mathbf{J} = \{\epsilon_i, \sigma_i, q_i\}$, taken from the OPLS force field[13] (Table 2) was also employed in the simulation for comparison purposes. The OPLS mixing rules

$$\epsilon_{ij} = (\epsilon_i\epsilon_j)^{1/2}; \qquad \sigma_{ij} = (\sigma_i\sigma_j)^{1/2} \quad (5)$$

were used with $\xi = 1$ for all of the sites.

The two sets of intermolecular parameters (**J** and **A**) have been used to construct four different models. In the first two models ($\mathbf{J}_r$ and $\mathbf{A}_r$), the benzene molecule is considered rigid and fixed in its equilibrium geometry. The intermolecular interaction energy, U^{inter}, is expressed by means of eqs 1 and 3, using the **J** and **A** set of parameters, respectively. Conversely, in models $\mathbf{J}_f$ and $\mathbf{A}_f$, molecular flexibility has been taken into account. In this case, the intramolecular energy is expressed as the usual sum of contributions from bond stretching, angle bending, and torsional motions:

$$E^{intra} = \sum_{i}^{bonds} k_i^b (r_i - r_i^0)^2 + \sum_{i}^{angles} k_i^a (\theta_i - \theta_i^0)^2 + \sum_{i}^{dihedrals} k_i^d (1 + \cos(n_i\phi_i + \gamma_i)) \quad (6)$$

The same set of intramolecular parameters $\{k^b, r_i^0\}$, $\{k^a, \theta_i^0\}$, and $\{k^d, n_i, \gamma_a\}$, reported in Table 1, was used for models $\mathbf{J}_f$ and $\mathbf{A}_f$, while **J** and **A** sets were employed to model the intermolecular interaction.

2.3. Computational Details. All simulations of the rigid models were performed on 108 molecules using a code based on the constraint method[41] to integrate the equation of motion. The runs of solid benzene have been carried out in the constant stress ensemble employing the Parrinello−Rahman[42] technique that allows the shape of the simulation cell to fluctuate. Equilibrium properties of the liquid phase have been studied in the NPT ensemble with the Nosé−Hoover thermostat and Andersen barostat,[43,44] while dedicated runs in the microcanonical ensemble have been adopted to study the dynamical properties. Long-range Coulombic interactions have been calculated with the Ewald sum scheme.[45] A time step of 5 fs was used throughout the runs.

All simulations with flexible models were performed with the parallel version of the Moscito 3.9[46] package, modified to take the ξ parameter into account. A system of 400 benzene molecules was simulated in the NPT ensemble, with $P = 1$ atm and different temperatures. Temperature and pressure were kept constant using the weak coupling scheme of Berendsen et al.,[47] setting the coupling times, τ_T and τ_P, at 0.75 and 1.38 ps, respectively.

During all runs the C−H bond lengths were maintained at their equilibrium value using the SHAKE algorithm,[48] and a time step of 1.5 fs was used. For both rigid and flexible models, the short-range intermolecular interactions have been truncated at $R_c = 11$ Å, employing the standard corrections for energy and virial.[1] Charge−charge long-range interactions were treated with the particle mesh Ewald (PME) method,[49,50] using a convergence parameter, α, of $5.36/2R_c$ and a fourth-order spline interpolation.

The calculated values of the thermodynamic and structural properties were compared with those of the available experimental data. Among them, the enthalpy of vaporization (ΔH^{vap}), defined as the difference between the enthalpy of the gas phase (H_g) and that of the liquid phase (H_l) at the temperature T, was calculated as

$$\Delta H^{vap}(T) = H_g(T) - H_l(T) \simeq RT - U_l(T) \quad (7)$$

where $U_l(T)$ is the interaction energy of the liquid. The positional correlation function (g_{inter}), which is comparable to recent neutron diffraction results,[18] was computed as

$$g_{inter}(r) = \frac{g_{CC}(r)}{4} + \frac{g_{HH}(r)}{4} + \frac{g_{CH}(r)}{2} \quad (8)$$

(40) Chandler, P. *STEPIT 7.7*; University of Oklahoma: Stillwater, OK, 1991.
(41) Ciccotti, G.; Ferrario, M.; Ryckaert, J. *Mol. Phys.* **1982**, *47*, 1253.
(42) Parrinello, M.; Rahman, A. *J. Appl. Phys.* **1981**, *52*, 7182.
(43) Nosè, S. *Prog. Theor. Phys.* **1991**, *103*, 1.
(44) Andersen, H. C. *J. Chem. Phys.* **1980**, *72*, 2384.
(45) Ewald, P. P. *Ann. Phys.* **1921**, *64*, 253.
(46) Paschen, D.; Geiger, A. *MOSCITO 3.9*; University of Dortmund, Dortmund, Germany, 2000.
(47) Berendsen, H. J. C.; Postma, J. P. M.; van Gunsteren, W. F.; Di Nola, A.; Haak, J. R. *J. Chem. Phys.* **1984**, *81*, 3684.
(48) Ryckaert, J. P.; Ciccotti, G.; Berendsen, H. J. C. *J. Comput. Phys.* **1977**, *55*, 3336.
(49) Darden, T.; York, D.; Pedersen, L. *J. Chem. Phys.* **1993**, *98*, 10089.
(50) Essmann, U.; Perera, L.; Berkowitz, M.; Darden, A.; Lee, H.; Pedersen, L. *J. Chem. Phys.* **1995**, *103*, 8577.

Table 1. Parameters Defining the Intramolecular Potential[a]

stretch	k_b (kJ mol^{-1} Å^{-2})	l^0 (Å)
C−C	2552.2	1.394
C−C (UB)	292.9	2.414
C−H	constrained	1.080
angle	k_a (kJ mol^{-1} rad^{-2})	θ^0 (deg)
C−C−C	334.72	120.0
C−C−H	251.04	120.0
dihedral	k_d (kJ mol^{-1})	γ (deg)
C−C−C−C	12.970	180.0
C−C−C−H	17.573	180.0
H−C−C−H	10.042	180.0

[a] All C−H bond distances were constrained to their equilibrium values. The C−C UB term refers to the Urey−Bradley stretching term (ref 3) in the dihedral energy (eq 6). All n values were set equal to 2.

where $g_{CC}(r)$, $g_{HH}(r)$, and $g_{CH}(r)$ are the standard atom−atom pair correlation functions.

Translational dynamics has been analyzed in terms of the center of mass mean square displacement (MSD), defined as

$$\mathrm{MSD} = \langle |\mathbf{r}(t) - \mathbf{r}(0)|^2 \rangle \tag{9}$$

and velocity autocorrelation function (acf), defined as

$$Z(t) = \frac{1}{3}\langle \mathbf{v}(t) \cdot \mathbf{v}(0) \rangle \tag{10}$$

The latter equation was used to compute the translational diffusion coefficient (D) as:

$$D = \int_0^\infty Z(t)\mathrm{d}t \tag{11}$$

Moreover, by projecting the $\mathbf{v}(t)$ vector onto the $\hat{C}_6$ and $\hat{C}_2$ axes of the benzene ring, one can observe the anisotropy of local translational dynamics.

In analogy with the above definitions, parallel ($\Theta_{||}$) and perpendicular ($\Theta_\perp$) rotational diffusion coefficients were also calculated as

$$\Theta_k = \int_0^\infty \langle \omega_k(t)\omega_k(0) \rangle \mathrm{d}t; \qquad k = ||,\perp \tag{12}$$

where $\omega_{||}$ and $\omega_\perp$ are the parallel and perpendicular projections, respectively, of the molecular angular velocity, ω, onto the $\hat{C}_6$ axis. For comparison with recent NMR results,[21] the reorientation of the $\hat{C}_6$ ($\hat{u}_{||}$) and $\hat{C}_2$ ($\hat{u}_\perp$) axes was also analyzed. This was only done for rigid models $\mathbf{J}_r$ and $\mathbf{A}_r$, where the ring plane is strictly defined, by calculating the time integral τ_k^l, defined as

$$\tau_k^l = \int_0^\infty \langle C_k^l(t) \rangle \mathrm{d}t; \qquad k = ||,\perp \tag{13}$$

where $C_k^1(t)$ and $C_k^2(t)$ are the first- and second-rank Legendre polynomial, respectively, of the function $\cos(\phi_k(t))$, with $\phi_k(t)$ being the angle between $\hat{u}_k(t)$ and $\hat{u}_k(0)$. The functions $\langle C_k^l(t) \rangle$, obtained by simulation runs, were fitted by the stretched exponential function (see ref 21 and references therein)

$$\langle C_k^l(t) \rangle_{\mathrm{fit}} = e^{(-t/\alpha_k^l)\beta_k^l} \tag{14}$$

whose time integral is analytical

$$\tau_k^l \simeq \int_0^\infty \langle C_k^l(t) \rangle_{\mathrm{fit}}\, \mathrm{d}t = \frac{\alpha_k^l}{\beta_k^l}\Gamma\left(\frac{1}{\beta_k^l}\right) \tag{15}$$

Table 2. ABD and OPLS Intermolecular Parameters Used in Rigid and Flexible Models $\mathbf{J}_r$ and $\mathbf{A}_r$, and $\mathbf{J}_f$ and $\mathbf{A}_f$, Respectively

	ABD (**A** set)	OPLS[a] (**J** set)
σ_C (Å)	3.42	3.55
ϵ_C (kJ mol^{-1})	0.347	0.293
ξ_C	1.14	1.00
q_C (e)	−0.126	−0.115
σ_H (Å)	2.93	2.47
ϵ_H (kJ mol^{-1})	0.021	0.125
ξ_H	1.34	1.00
q_H (e)	0.126	0.115
RMS (kJ mol^{-1})	1.6	7.5
Q^b (C m^2)	24.5×10^{-40}	23.3×10^{-40}

[a] From ref 15. [b] The electric quadrupole moment (Q) resulting from the fitted point charges. The experimental value (ref 32) of Q is $(29.0 \pm 1.7) \times 10^{-40}$ C m^2.

Finally, the shear (η_S), longitudinal (η_L), and bulk (η_B) viscosities were calculated from the time integral of the correlation function of the proper elements of the stress tensor ($\hat{\sigma}$).

$$\eta_S = \frac{V}{6k_BT}\int_0^\infty \sum_{\alpha=1}^{3}\sum_{\beta\neq\alpha}^{3} \langle \sigma_{\alpha\beta}(0)\sigma_{\alpha\beta}(t) \rangle \mathrm{d}t \tag{16}$$

$$\eta_L = \frac{V}{3k_BT}\int_0^\infty \sum_{\alpha=1}^{3} \langle \sigma_{\alpha\alpha}(0)\sigma_{\alpha\alpha}(t) \rangle \mathrm{d}t \tag{17}$$

$$\eta_B = \eta_L - \frac{4}{3}\eta_S = \frac{V}{9k_BT}\int_0^\infty \sum_{\alpha,\beta=1}^{3} \langle \sigma_{\alpha\alpha}(0)\sigma_{\beta\beta}(t) \rangle \mathrm{d}t \tag{18}$$

3. Results and Discussion

3.1. Ab Initio-Derived (ABD) Potential. The PES of the benzene dimer has been sampled through the ab initio MP2 computation[10,23] of the interaction energy for 197 different geometries (N_{geom}), and the resulting database[23] was fitted with the full atomic model potential described in 2.2, which from now on will be referred to as the ab initio-derived (ABD) potential. The weighting function, w, that appears in eq 4 is chosen in order to improve the fit of the potential

$$w_k = e^{-\alpha E_k}$$

where E_k is the ab initio computed energy in the kth dimer configuration, and α was set to 3.5 kJ/mol, corresponding to the Boltzmann factor at ∼600 K.

The parameters of both ABD and OPLS model potentials are reported in Table 2, together with the RMS values and the quadrupole moments generated by the atomic charges.

In Figure 1 some paradigmatic arrangements of the benzene dimer are sketched: T-shaped (TS), face to face (FF), cross (CR), side by side (SS), and slipped parallel (SP). These geometries are shown in Figure 2, where the ABD intermolecular potential is compared with the ab initio energies and the OPLS.[15]

It is apparent that the two curves in Figure 2 show a marked resemblance in all of the considered geometries, with some differences near the bottom of the wells, where the OPLS potential is generally more negative. The different RMS values of the two potentials (1.6 and 7.5 kJ/mol for ABD and OPLS, respectively; see Table 2) are due to large differences for some repulsive energies at small interatomic distances. Figure 2 shows that the inclusion of the ξ parameter, which allows one to

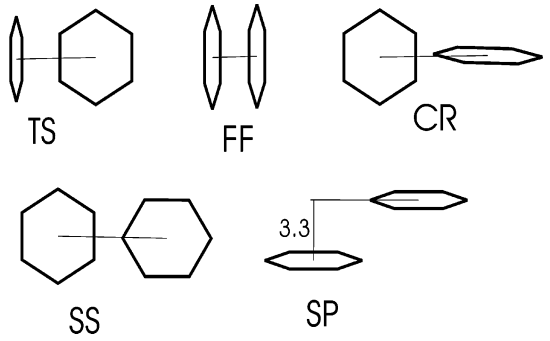

Figure 1. Typical arrangements for the benzene dimer. The 3.3 Å value refers to R_1 (see Figure 2).

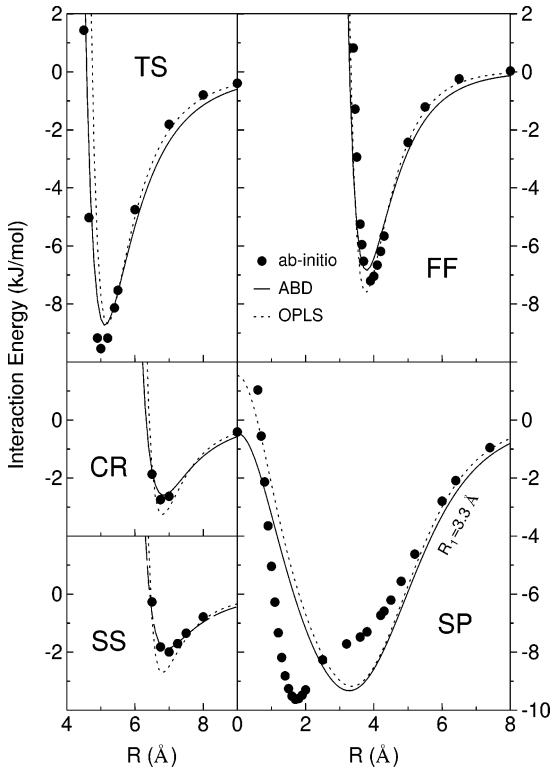

Figure 2. Intermolecular energies for the benzene dimer in some typical arrangements: ABD potential (—), MP2 energies (●), OPLS potential (- - -). The geometrical arrangements correspond to those reported in Figure 1.

modulate the slope of the curve around $r = \sigma$, leads to a satisfactory reproduction of the repulsive region.

Considering the different origin of these potentials (the OPLS force field was adjusted to reproduce the experimental density and enthalpy of vaporization), their remarkable agreement is gratifying. Indeed, since the OPLS force field has proven to give accurate results in a variety of applications,[15,20,21] this agreement reinforces the reliability of both ABD and OPLS force fields.

From Figure 2, it is also apparent that the ab initio energy data in both model potentials are generally able to be reproduced with reasonable accuracy. However, some discrepancies remain around the bottom of the wells and in the SP arrangement. This clearly indicates that, for some conformations, these simple model potentials may be inadequate for reproducing the complex shape of the QM PES, and more versatile functional forms should be designed in order to reinforce the link between ab initio calculations and simulated bulk properties.

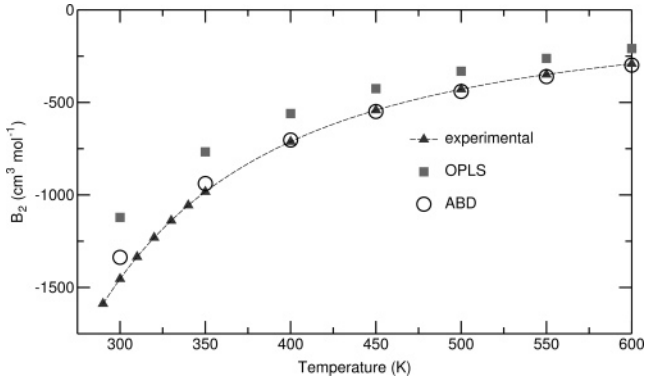

Figure 3. Second virial coefficient vs temperature. Comparison between experimental (refs 28 and 36) and theoretical results obtained by ABD and OPLS potentials.

Comparing the parameters of the two potentials (Table 2), we observe that some differences stand out clearly, particularly for the parameters of the H atoms. However, the redundancy of the atom−atom functions and the effect of the ξ value make a parameter-to-parameter comparison rather questionable. In fact, the two potentials turn out to be very close to each other. Finally, the larger absolute value of the ABD point charges, q_i, yields an overall quadrupole moment slightly closer to the experimental value of $(29.0 \pm 1.7) \times 10^{-40}$ C m^2, obtained with birefringence measurements.[32]

A first test on the quality of the ABD and OPLS potentials has been carried out through the calculation of the second virial coefficient

$$B_2(T) = -\frac{N_A}{2}\int \mathrm{d}\mathbf{r} \int \mathrm{d}\Omega\, [e^{-U\mathrm{inter}(\mathbf{r},\Omega)/k_B T} - 1] \quad (19)$$

whose results are displayed in Figure 3.

The agreement with the experimental data seems to indicate that both models are able to correctly reproduce the main features of the benzene−benzene interaction. In particular, our potential is in quantitative accord with the experimental results beyond $T = 400$ K, with increasing deviations at lower temperatures. This confirms the overall quality of the ab initio calculations and the accuracy of the fitting. At the same time, there is still room for improvement in the description of the most-attractive regions of the PES. On the other hand, a worse performance of the OPLS model, for observations deriving directly from the two-body potential (i.e., B_2), should be expected since it was designed to reproduce condensed-phase properties.

3.2. Simulation Results. The initial configuration was set by placing four molecules per unit cell with the experimental geometry of the benzene crystal.[26] This unit cell was replicated three times along each axis of the simulation box, obtaining, in such a way, a system of 108 rigid molecules. Conversely, to obtain a lattice structure of 400 flexible molecules, the unit cell was replicated five, four, and five times along the *x*, *y*, and *z* direction, respectively.

This low-pressure experimental orthorhombic structure was used as a starting configuration for all runs. Figure 4 presents an overview of the results of our temperature scan as far as enthalpy and density of the flexible models are concerned. More comprehensive and detailed information is provided in the following.

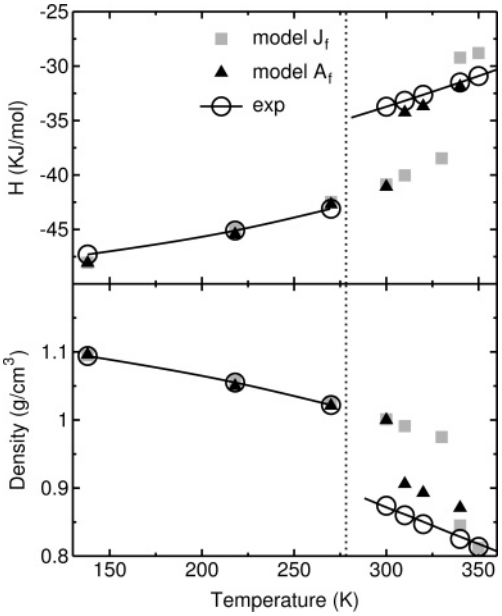

Figure 4. Enthalpy H and density as a function of temperature for the flexible models. Specific heat at constant pressure and thermal expansion coefficients were determined from the slope of the resulting curves for the two models. The dotted vertical line indicates the experimental melting temperature (278.6 K).

Benzene Crystals. For all of the models, the behavior of the system was investigated at several temperatures in the solid phase with runs of more than 1 ns and the external pressure being fixed at 1 atm.

Cell parameters, as well as density and intermolecular energies for the crystals, are reported in Table 3. As can be seen, all of the models yield results that are in good agreement with experimental data, with the flexible models providing an improvement with respect to the rigid ones.

The all-atom representation employed here allows us to obtain a better description of the lattice parameters with respect to the simplified, single-site model of ref 23, except for the molecular orientation. The latter was found to be in quantitative agreement, with the experimental data at 100 K, with our parametrization of the Gay−Berne model on the same set of ab initio data used in the present work. Also, the temperature dependence of the angles, which specify the orientation of molecule **I** in the unit cell, is correctly reproduced by the adopted potentials. As Figure 2 shows, the TS and SP configurations of the dimer have almost equal energies. Apparently, packing effects of the crystal phase do not significantly affect these favorite arrangements as there are near neighbors of both kinds,[26] whereas FF configurations are found for more distant pairs of molecules.

For rigid model $\mathbf{J}_r$, the ordered phase was stable up to 310 K, where melting was observed after 350 ps, while for model $\mathbf{A}_r$, melting occurred at 275 K in 700 ps. When the constraint of the fixed internal geometry was relaxed, the melting temperature increases to 340 K with model $\mathbf{J}_f$ and to 310 K with model $\mathbf{A}_f$, with runs of 0.5 and 1.5 ns, respectively. In particular, the crystalline structure of model $\mathbf{J}_f$ remains stable at 320 K for more than 4 ns. Also, from this point of view, the present models outperform the single-site ones,[23] which predict melting temperatures, at best, in qualitative agreement with the experimental data.

Thermodynamic Properties. The average densities and internal energies of the equilibrated systems, reported in Figure 4, were calculated as a function of temperature. The thermal expansion coefficient (α) and the constant pressure specific heat (c_p) have been calculated from the slope of the density or enthalpy versus the temperature curve, while the melting enthalpy (ΔH^m) has been estimated from the jump of the enthalpy curve (Figure 4). These thermodynamic properties of the model benzene are compared with the relevant experimental data in Table 4 at 300 K, which is a temperature corresponding to a supercooled liquid for all of the models except $\mathbf{A}_r$.

As expected, model $\mathbf{J}_r$ reproduces, quantitatively, both experimental density (ρ) and enthalpy of vaporization (ΔH^{vap}) as the OPLS parameter set was adjusted to reproduce these properties. Our result for the density of model $\mathbf{A}_r$ overestimates the experimental data at all of the temperatures explored (Table 5), with minor differences in ΔH^{vap}. Most importantly, from our point of view, the $\mathbf{A}_r$ system melts at a temperature very close to the experimental one, though the melting enthalpy is significantly underestimated.

The major effect of relaxing the internal degrees of freedom is an increase of density and melting temperature, registered for both $\mathbf{J}_f$ and $\mathbf{A}_f$. On the contrary, minor differences were obtained for melting and vaporization enthalpies. No clear effect is visible on the fluctuation quantities, α and c_p, if one considers the large uncertainty on these results. The latter, in particular, is much smaller than the experimental value for all rigid and flexible models. The result we obtain with model $\mathbf{J}_r$ differs significantly from that reported in ref 15, which was in quantitative accord with the experimental value. This point has been further investigated by performing a Monte Carlo run at constant T (298 K) and P (1 atm) with the BOSS[51] program. After a run of more than 50 million configurations, we found again a c_p of 80 ± 5 J mol^{-1} K^{-1}, which was in agreement with MD results on the same $\mathbf{J}_r$ model. The different number of molecules (142 vs 128 of ref 13) and C−H bond lengths (1.395 vs 1.400 Å of ref 15) appear too small to justify the observed discrepancy of heat capacities.

Liquid Benzene Structure. To obtain a completely isotropic phase, the two flexible models were heated at 340 K for 0.5 ns. The configurations obtained were cooled to 300 K in four steps of 10 K each, with runs of 0.2 ns. The systems obtained were then equilibrated for another 1.5 ns.

Both flexible models turned into a liquid at 300 K after these procedures were completed, with a density of 0.893 and 0.911, respectively (Table 4). The structure of the systems was characterized by calculating $g_{inter}(r)$ from the relevant atom−atom pair correlation functions, $g_{CC}(r)$, $g_{CH}(r)$, and $g_{HH}(r)$, according to eq 8.

Comparison of the latter with the one resulting from neutron diffraction measurements[18] is reported in Figure 5. Both models give results that agree satisfactorily with the experimental data, with the $\mathbf{A}_f$ being slightly closer to the experimental $g_{inter}(r)$ for r up to ≃8 Å. There is still a minor discrepancy between the simulations and experimental data in the description of the first peak and in the period of the oscillations.

In conclusion, the performance of the **A** models on the thermodynamic and structural properties well compares with that of the $\mathbf{J}_f$ and $\mathbf{J}_r$ models, which have been constructed on the basis of such properties.

(51) Jorgensen, W. *BOSS 4.2*; Yale University: New Haven, CT, 2001.

Table 3. Calculated and Experimental[a] Crystal Data at 138, 218, and 270 K[b]

model	T (K)	U (kJ mol^{-1})	ρ (g cm^{-3})	a (Å)	b (Å)	c (Å)	θ[c]	φ[c]	ψ[c]
$\mathbf{J}_r$	138	−47.5 ± 0.85	1.086 ± 0.0010	7.30	9.39	6.81	0.86 ± 0.02	0.23 ± 0.02	1.84 ± 0.05
$\mathbf{A}_r$	138	−47.2 ± 0.77	1.063 ± 0.0010	7.49	9.18	7.10	0.87 ± 0.01	0.37 ± 0.04	1.20 ± 0.02
$\mathbf{J}_f$	138	−48.0 ± 0.08	1.099 ± 0.0006	7.27	9.35	6.94			
$\mathbf{A}_f$	138	−48.1 ± 0.09	1.095 ± 0.0008	7.34	9.23	6.98			
exp	138	−47.3	1.094	7.39	9.42	6.81	0.82	0.36	1.52
$\mathbf{J}_r$	218	−43.4 ± 0.52	1.030 ± 0.0010	7.43	9.53	7.11	0.88 ± 0.02	0.09 ± 0.26	1.52 ± 0.17
$\mathbf{A}_r$	218	−43.7 ± 0.52	1.014 ± 0.0010	7.61	9.25	7.27	0.88 ± 0.02	0.05 ± 0.26	1.22 ± 0.07
$\mathbf{J}_f$	218	−44.9 ± 0.18	1.060 ± 0.0019	7.24	9.51	7.10			
$\mathbf{A}_f$	218	−45.4 ± 0.12	1.055 ± 0.0050	7.38	9.35	7.09			
exp	218	−45.1	1.055	7.44	9.55	6.92	0.83		
$\mathbf{J}_r$	270	−41.4 ± 0.66	1.007 ± 0.0010	7.35	9.70	7.24	0.89 ± 0.03	0.10 ± 0.35	1.56 ± 0.14
$\mathbf{J}_f$	270	−42.5 ± 0.19	1.028 ± 0.0020	7.25	9.67	7.20			
$\mathbf{A}_f$	270	−42.7 ± 0.13	1.021 ± 0.0013	7.42	9.57	7.14			
exp	270	−43.1	1.022	7.46	9.66	7.03	0.84	0.31	1.54

[a] From refs 25 and 26. [b] No data are reported for the $\mathbf{A}_r$ model at 270 K as the onset of the melting process produces severe distortions of the cell shape. [c] The Eulerian angles, θ, φ, and ψ (radians), define the orientation of molecules of type I in the elementary cell.

Table 4. Experimental and Calculated Thermodynamic Properties[a]

	exp	$\mathbf{J}_r$	$\mathbf{A}_r$	$\mathbf{J}_f$	$\mathbf{A}_f$
ρ	0.874[b]	0.873	0.900	0.893 ± 0.003	0.911 ± 0.005
α	1.198[c]	1.56 ± 0.16	1.02 ± 0.13	1.35 ± 0.11	1.14 ± 0.13
c_p	135.69[d]	84 ± 8	59 ± 7	64 ± 9	83 ± 8
T_m	278.64[b]	310	275	340 ± 10	310 ± 5
ΔH^m	9.3[e]	8.8 ± 0.8	5.2 ± 0.6	8.4 ± 0.8	6.6 ± 0.6
ΔH^{vap}	33.92[f]	33.6 ± 0.4	36.3 ± 0.38	34.9 ± 0.23	36.9 ± 0.25

[a] Density ρ (g cm^{-3}), thermal expansion coefficient α ($\times 10^{-3}$ K^{-1}), c_p (J mol^{-1} K^{-1}), and ΔH^{vap} refer to the liquid at 298 K. (Temperatures are in K and enthalpies in kJ mol^{-1}.) [b] From ref 36. [c] From ref 35. [d] From ref 34. [e] From ref 31. [f] From ref 33.

Table 5. Experimental[a] and Calculated Translational Diffusion Coefficients and Densities

model	T (K)	ρ (g cm^{-3})	D ($\times 10^5$ cm^2 s^{-1})
$\mathbf{J}_r$	281	0.905	1.05
$\mathbf{A}_r$	278	0.925	1.15
$\mathbf{J}_f$	283	0.905	1.2 ± 0.16
$\mathbf{A}_f$	280	0.928	1.5 ± 0.11
exp	288	0.885	1.90
$\mathbf{J}_r$	303	0.870	1.95
$\mathbf{A}_r$	301	0.900	2.00
$\mathbf{J}_f$	300	0.885	1.7 ± 0.13
$\mathbf{A}_f$	300	0.902	2.1 ± 0.12
exp	298	0.874	2.27
$\mathbf{J}_r$	312	0.857	2.15
$\mathbf{A}_r$	328	0.873	2.70
$\mathbf{J}_f$	320	0.865	2.6 ± 0.07
$\mathbf{A}_f$	320	0.883	2.9 ± 0.10
exp	318	0.852	2.68

[a] From ref 27.

Single-Particle Dynamic Properties. A demanding test, for all models, is the reproduction of the experimental dynamic properties. To investigate the dynamical behavior, the system in its liquid state was equilibrated in the NPT ensemble at 288, 298, and 318 K.

For both rigid models, several simulation runs of 100 ps each were then performed in the NVE ensemble to calculate translational and rotational diffusion coefficients, which are reported in Tables 5 and 6, respectively.

For the flexible models, the liquid phase, obtained as described above, was first equilibrated to the desired temperature through an NPT run of 1 ns. The equilibrated system was then constrained in a box of constant volume. Four short NVE runs of 10 ps each were performed with both flexible systems,

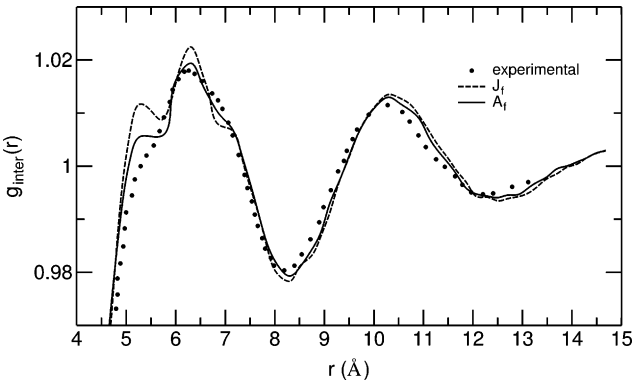

Figure 5. Intermolecular pair correlation function obtained from the atom−atom functions compared to the g_{inter} obtained from neutron diffraction measurements (ref 18).

Table 6. Experimental and Calculated Rotational Diffusion Coefficients, Θ_k ($\times 10^{10}$ rad^2 s^{-1}), and Axis Reorientation Times, τ_k^j (ps)

model	T (K)	$\Theta_\parallel$	$\Theta_\perp$	$\tau_\parallel^1$	$\tau_\perp^1$	$\tau_\parallel^2$	$\tau_\perp^2$
$\mathbf{J}_r$	281	18.5	8.5	7.1	4.1	2.3	1.6
$\mathbf{A}_r$	278	27.0	8.5	7.5	3.2	2.4	1.4
$\mathbf{J}_r$	303	23.0	12.5	4.7	3.0	1.6	1.2
$\mathbf{A}_r$	301	35.0	12.4	5.4	2.6	1.6	1.1
exp[a]	300	15.9−28.8	7.4−10.2				0.94−1.3
$\mathbf{J}_r$	312	29.0	16.0	3.5	2.5	1.2	1.0
$\mathbf{A}_r$	328	43.0	16.5	3.8	2.0	1.2	0.9

[a] From ref 21.

averaging the time correlation functions over all of the relevant trajectories. The resulting coefficients, D, are reported in Table 5.

As can be seen from Table 5, the translational diffusion in liquid benzene is slightly underestimated by all of these models. For the $\mathbf{J}_r$ model, this seems to be a known deficiency, already found by other authors.[21] **A** models, especially $\mathbf{A}_f$, are closer to the experimental values, in particular, at higher temperatures. The enhancement of translational diffusion, due to the introduction of flexibility, is a feature shared by both **J** and **A** models.

It is worth noticing that the short time behavior of the velocity acf shows, for both models, a difference if projected along a parallel or perpendicular direction to the $\hat{C}_6$ axis. In the short time regime, in fact, benzene is more likely to diffuse in the plane of the ring as a consequence of local anisotropy, produced by the short range order around the tagged molecule.

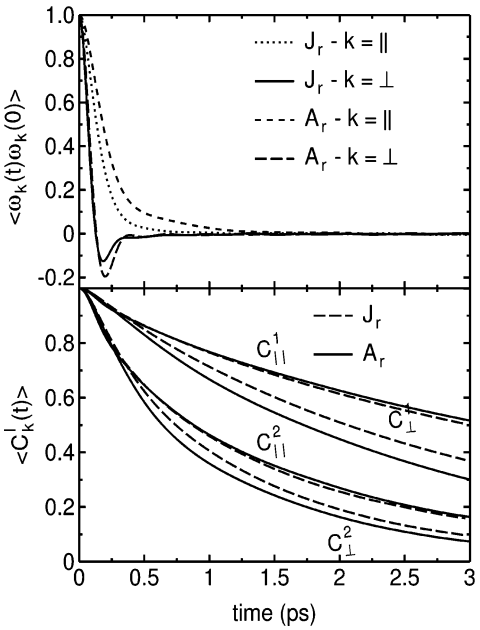

Figure 6. Correlation function for the rotational diffusion in rigid models at 300 K. In the top panel, the normalized angular velocity correlation functions are reported, while axis reorientation is shown in the bottom panel.

From the angular velocity autocorrelation function, the parallel and perpendicular ($\Theta_{||}$ and $\Theta_{\perp}$) rotational diffusion coefficients have been calculated as shown in eq 12. The symmetry axes' reorientation times (τ_k^l, with $l = 1$ or 2 and $k = ||,\perp$) were obtained from the correlation of the $\hat{C}_6$ and $\hat{C}_2$ axes (eq 15). Both correlation functions are reported in Figure 6 for the rigid models. Note that since the reorientation of the $\hat{C}_6$ axis is due to rotation around the $\hat{C}_2$ axes, the $\Theta_{||}$ values are to be connected to the $\tau_{\perp}^l$ times and vice versa.

From Table 6, it can be noted that the rotation about the $\hat{C}_2$ axes, namely, the reorientation of the $\hat{C}_6$ axis, is described by both models much the same way and compares fairly well with the experimental values. On the contrary, though the experimental results are rather scattered,[21] rotation about the $\hat{C}_6$ axis seems to be overestimated by model $\mathbf{A}_r$. However, this overestimation does not lead to an incorrect value of $\tau_{\perp}^2$, which indeed is well within the experimental range. As a consequence, the value of the rotational anisotropy of model $\mathbf{A}_r$ ($\sigma_R = \Theta_{||}/\Theta_{\perp}$) of 2.8 is still consistent with the experimental values[21] ($\sigma_R \simeq 1.6-2.9$).

Since both translational and rotational diffusions are thermally activated processes, one can calculate the relevant activation energies from the Arrhenius expressions.

$$D(T) = D_0\, e^{-E^{tr}_a/RT}$$

and

$$\Theta_i(T) = \Theta_{0i}\, e^{-E^{rot}_{ai}/RT}; \qquad i = ||,\perp$$

or

$$\tau_i(T) = \tau_{0i}\, e^{E^{rot}_{ai}/RT}$$

The results shown in Table 7 confirm that translational dynamics is satisfactorily described by all of the models, while the $\mathbf{J}_r$ model performs better in modeling rotational dynamics around the $\hat{C}_6$ as well as $\hat{C}_2$ axis.

Table 7. Experimental and Calculated Activation Energies for the Translational and Orientational Diffusion

model	E_a^{tr} (kJ mol^{-1})	$E_{a||}^{rot}$ (kJ mol^{-1})	$E_{a\perp}^{rot}$ (kJ mol^{-1})
$\mathbf{J}_r$	16.0	11.3	8.1
$\mathbf{A}_r$	12.7	9.9	6.6
$\mathbf{J}_f$	13.5		
$\mathbf{A}_f$	14.2		
exp	13.0[a]	13.3[b]	8.2[b]

[a] From ref 27. [b] From ref 21.

Table 8. Experimental and Calculated Viscosities

model	T (K)	η_S (cP)	η_B (cP)
$\mathbf{J}_r$	277	0.79 ± 0.080	0.49 ± 0.044
$\mathbf{A}_r$	278	0.84 ± 0.024	0.39 ± 0.066
exp[a]	283	0.76	
$\mathbf{J}_r$	303	0.58	0.41
$\mathbf{A}_r$	301	0.57 ± 0.024	0.18 ± 0.002
exp[a]	303	0.56	
$\mathbf{A}_r$	328	0.46 ± 0.020	0.24 ± 0.03

[a] From ref 29.

Viscosities. Benzene collective dynamics has been studied by calculating the various viscosities according to the Green−Kubo relations (eqs 16−18). This analysis has been restricted to rigid models for computational convenience. The results obtained at different temperatures are shown in Table 8. The uncertainty of these data has been estimated by averaging the various runs, namely, 3 at 278 K and 2 at 301 and 328 K, each 0.5 ns long.

Both models appear to satisfactorily reproduce the experimental results of shear viscosity at $\simeq$ 300 K. Measurements of bulk viscosity are more scarce. However, according to a recent study of acoustic relaxation time,[37] η_B should not exceed 0.36 η_S (i.e., $\simeq$ 0.23 cP at 300 K). This result is closer to the data of model $\mathbf{A}_r$ than to that obtained with the $\mathbf{J}_r$ potential. Larger values of bulk viscosity (at least as large as shear viscosity) have been reported by Luo and Hoheisel[52] in a MD study of a six-center model of benzene at various temperatures.

In the same paper, a long-time tail in the integrand of shear viscosity has been observed, whose contribution to the transport coefficient increases at lower temperatures. An analogous behavior is shown in Figure 7 where the normalized stress tensor acf is compared to the angular velocity acf for rotation around the $\hat{C}_2$ axes, at $T = 278$ K. Both functions share an initial, rapidly decaying oscillatory part that is superseded by the long-time tail in the stress tensor acf. The latter contribution to the integral is very slowly fading away, so that the value reported in Table 8 has actually been obtained from a fit according to the following expression:

$$\int_0^t \mathrm{d}s\langle\sigma_{\alpha\beta}(0)\sigma_{\alpha\beta}(s)\rangle = a_1(1 - e^{-t/\tau_1}) + a_2(1 - e^{-t/\tau_2}) \quad (20)$$

Luo and Hoheisel[52] have related the long-time tail of the stress tensor acf to the second-order reorientational acf (Figure 6). At 278 K, the relaxation time of the slow exponential of eq 20 (3.7 ps) is actually fairly larger than that of the second-order reorientational acf (2.4 ps). This increase, however, might be due to collective effects on rotational dynamics. Model $\mathbf{A}_r$ also

(52) Luo, H.; Hoheisel, C. *Phys. Rev. A* **1991**, *44*, 6421.

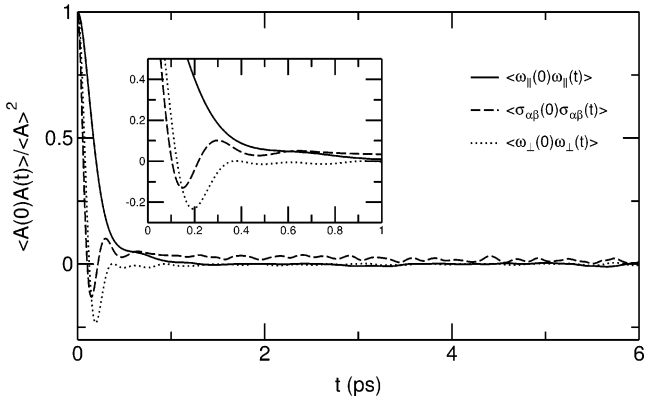

Figure 7. Comparison of normalized spinning ($\omega_{\parallel}$) and tumbling ($\omega_{\perp}$) angular velocity correlation functions with the shear viscosity integrand ($\langle\sigma_{\alpha\beta}(0)\sigma_{\alpha\beta}(t)\rangle$; see eq 16). Inset shows details of the short time region (T= 278 K).

seems to qualitatively account for the temperature dependence of viscosity, although the overestimated value at 278 K (i.e., close to the melting point) might be due to an overestimated density (0.925 vs 0.890 g/cm^3).

4. Summary and Conclusions

The main goal of this paper was to test the possibility of obtaining intermolecular potentials suitable for computer simulation on the basis of quantum chemical calculations, with no recourse to experimental data.

To this end (and to keep the paper within manageable length), we preferred to examine several diverse properties, rather than exploiting the wealth of detailed information provided by MD to gain insight into the physics underlying the results.

The ab initio scheme adopted (MP2 with double-ζ plus polarization basis set) has proven to be accurate enough to provide results in good agreement with the most-reliable theoretical values available for the minimum interaction energy of the dimer. This accuracy has been confirmed by the calculated second virial coefficient, which shows minor deviations from the experimental values only at the lowest temperatures explored.

The measured values of density and internal energy of the crystal are well reproduced. In all cases, relaxing the internal degrees of freedom improves the reproduction of experimental data.

Rigid and (more so) flexible **A** models overestimate the liquid-phase density by $\simeq$3% and ΔH^{vap} by $\simeq$10%. As expected, the latter properties are quantitatively reproduced by the $\mathbf{J}_r$ model, which was parametrized on these data, but slightly overestimated by the $\mathbf{J}_f$ model. Melting temperature of real benzene (278.6 K) is better predicted by the $\mathbf{A}_r$ (275 K) than the $\mathbf{J}_r$ model (310 K), while both flexible models are off by about +40 and +60 K, respectively. Moreover, all models give good results for the thermal expansion coefficient, but they largely underestimate heat capacity at 300 K.

The total radial distribution function derived from neutron diffraction measurements at 300 K is well reproduced by $\mathbf{A}_f$ and $\mathbf{J}_f$ models, with negligible differences between them.

The translational diffusion coefficient is generally underestimated, with a small improvement due to flexibility. Larger differences between the **J** and **A** models are apparent in modeling rotational and reorientational dynamics, especially as far as rotation around the $\hat{C}_6$ axis is concerned. In the latter case, **A** models yield rotational diffusion coefficients larger than those of the **J** models and slightly out of the range of the relevant experimental data.

$\mathbf{A}_r$ and $\mathbf{J}_r$ models are able to quantitatively reproduce the experimental data of shear viscosity at 300 K, and also, the large increase of shear viscosity observed at lower temperatures is satisfactorily accounted for by both rigid models. The predicted bulk viscosity of the $\mathbf{J}_r$ model (0.41 cP) is twice as large as that of $\mathbf{A}_r$ (0.18 cP). The latter value is supposed to be in closer agreement with recent estimates of bulk viscosity ($\leq$0.23 cP).

The overall picture emerging from this summary shows that a simple LJ + Q potential, with the parameters derived by Jorgensen and Severance, is able to describe in a semiquantitative way a variety of structural and dynamical properties of solid and liquid benzene. It is worth stressing that this success extends well beyond the properties and the thermodynamic conditions adopted in the parameter optimization process.

Our model matches the performance of the **J** model in most cases, with some weaker (density, vaporization enthalpy, and rotational dynamics around the $\hat{C}_6$ axis) and some stronger points (second virial coefficient, melting temperature, and bulk viscosity).

Adding a description of the intramolecular interactions with the CHARMM force field affects the results of the **A** and **J** models to almost the same extent. Molecular flexibility improves some results, however, others are worsened (noticeably, density) so that rigid models are to be preferred for benzene, in our opinion, unless one is particularly interested in its internal dynamics.

Our attention to benzene is mainly due to the presence of the phenyl ring in many liquid−crystal-forming molecules. Hence, the results described here, combined with the remarkable accuracy of the reconstruction of the interaction potential of large molecules[38] from that of their constitutive fragments (e.g., benzene) allow us to pursue this approach to force fields with some confidence.

JA046642U